

Lithic artifacts and texture analysis: a low magnification approach

Guillermo Bustos-Pérez^{1,2,3} Andreu Ollé^{2,3}

¹Universidad Autónoma de Madrid. Departamento de Prehistoria y Arqueología, Campus de Cantoblanco, 28049 Madrid, Spain.

²Institut Català de Paleoecologia Humana i Evolució Social (IPHES), Zona Educacional 4, Campus Sesce-lades URV (Edifici W3), 43007 Tarragona, Spain.

³Àrea de Prehistòria, Universitat Rovira i Virgili (URV), Avinguda de Catalunya 35, 43002 Tarragona, Spain.

Abstract

Lithic artifacts are some of the most common and numerous remains from paleolithic archaeological sites. However, their deposition into the archaeological record can be the result of multiple episodes of discard which are

Because the numerous amount of lithic remains, a quick, flexible, low cost and effective method for identifying degrees of alteration in the surface of lithic implements is highly desirable. This would favor the analysis of complete lithic assemblages, inferring their overall integrity, identify different episodes or clusters of alteration, and even identify post-depositional alterations of different nature (such as rounding, dragging or wind erosion).

An experimental collection of flints and quartzites were subjected to sequential episodes of rounding. After each episode, photographs with a Dino-Lite Edge 3.0 AM73915MZT USB microscope were taken, allowing to obtain quantitative values of surface texture. Following this, the quantitative data of surface texture was employed as variables in Machine Learning models to determine degree of rounding and the most important variables for discrimination.

Results show, that despite being a continuum,

Key words: experimental archaeology; postdepositional alterations

1. Introduction

Lithic artifacts constitute one of the most common remains from paleolithic archaeological sites. When analyzing a lithic assemblages, a key factor to consider is determining the degree of post-depositional alterations undergone by the assemblage since this results in behavioral and eco-cultural inferences. Methods for determining assemblage integrity usually focus on the assemblage as a hole. These methods often include spatial analysis of artifacts and analysis of fabrics to determine if water flow has resulted in a reorganization of the spatial distribution ([Lenoble and Bertran, 2004](#); [McPherron, 2005](#); [McPherron, 2018](#); [Petraglia and Potts, 1994](#); [Schick, 1987](#)). Also lithic size distribution analysis are realized to determine if postdepositional processes have resulted in sorting of the materials ([Bertran et al., 2012](#); [Maíllo Fernández, 1998](#); [Schick, 1987](#)). Another option is to focus directly on individual lithic artifacts to determine the degree of alteration that they have undergone ([Chu et al., 2015](#); [Levi Sala, 1986](#)). Although being more time consuming, this type of analysis provides a higher resolution, allowing to establish a graduation in the degree of postdepositional alterations, to combine its data with spatial analysis, dissecting archaeological episodes, or to detect several episodes of recycling.

Individually determining the degree of alteration undergone by a lithic artifact uses microscopic analysis to measure ridge width, visually analyze the surface to determine the existence and intensity of abrasion, and examine the edges to determine the presence of detachments coming from particle impact or dulling of the edges in more extreme cases ([Bustos-Pérez et al., 2019](#); [Chambers, 2003](#); [Shackley, 1974](#)). Of these measures, ridge width is the most clearly quantifiable which can result in a greater weight on the analyst's decision. However, analysis from sequential experimentations shows that the longer the exposure time to sedimentary abrasion, greater the increase in the standard deviation of ridge width measurements ([Bustos-Pérez et al., 2019](#)). This introduces a degree of uncertainty when determining the degree of rounding undergone by a stone tool, since the ratio of increasing ridge width might be the result of general flake topography, ridge position among the flake, ridge angle, or general profile of the ridge.

Adding to the variability in flake width (which comes from flake and ridge morphology), it is also necessary to consider the effects of fluvial sedimentary processes which commonly affect lithic artifacts. Fluvial sedimentary processes are characterized by particle transport and these processes are not homogeneous. Lithic artifacts can form part of these process as another particle or remain static and be affected by the particles forming part of them. Commonly, three modes of particle transport are described in fluvial sedimentary contexts: rolling, sliding and saltation ([Alhusban and Valyrakis, 2021](#)), although the last one is not a common form of alteration in the case of stone tools ([Schick, 1986](#)). Additional to alterations coming from fluvial contexts, stone artifacts might also be affected by aeolian particle transport, usually resulting in wind erosion [Stapert \(1976\)](#).

Stone tools have an additional factor of variability added to the ones derived from particle transport and sedimentary contexts (fluvial or eolian). This additional factor comes from the degree of exposure and speed on which a stone tool enters the archaeological record ([Petraglia and Potts, 1994](#); [Schick, 1986](#); [Schiffer, 1972](#)). For example, it is expected that partially buried artifacts with water and sediment flowing above them will present modifications in the exposed surface, while edges and the burred surface will remain semi-intact ([Petraglia and Potts, 1994](#)). A different scenario happens when artifacts are transported by rolling in coarse sediments, resulting in abrasion of all surfaces, dulling of the edges, but at the same time, the impact from coarse particles might result in freshly detached surfaces and edges which undergo new modifications until the artifact enters the archaeological record ([Harding et al., 1987](#); [Petraglia and Potts, 1994](#)).

Thus, obtaining quantitative data of surface modifications can complement values of ridge width, and help identify and interpret type of particle transport undergone by, or affecting a stone artifact. Ideally, quantitative values of surface abrasion would be extracted from each stone artifact, allowing to maximize information and interpretation of the formation process of an archaeological site. However, as previously mentioned, stone artifacts are some of the most common remains from Paleolithic archaeological sites. Thus, a versatile, fast and non-time consuming method is highly desirable since it would enable to analyze large quantities of lithic materials.

This research presents results from a sequential experimentation in which a set of experimentally knapped flakes have undergone rounding process in a tumbler. After each episode of rounding, the same areas are photographed, and quantitative measures of flake texture are employed to characterize the surface. Following the extraction of quantitative values, Machine Learning models are employed to determine the degree of separation between rounding times. Flake ridge width is also considered as an indicative measure of alteration undergone by flakes.

2. Methods

2.1 Experimental sample

Three blocks of flint representing three different types (F1, F2 and F3) and three blocks of quartzite also representing three different types (Q1, Q2 and Q3) were experimentally knapped. Flint type F1 is characterized by a heterogeneous grey color surface with intrusions of geodes. Types F2 and F3 present a much more homogeneous surface, with colors being blue/grey and reddish/ocher. The three types correspond to the South Madrid Miocene Flint (SMM; [Bustillo and Pérez-Jiménez \(2005\)](#); [Bustillo et al. \(2012\)](#)) although

their locations varied widely. Quartzite type Q1 was collected at the Jarama river (Madrid, Spain) and it is characterized by a semi-fine grained surface of light blue/grey color. Quartzites types Q2 and Q3 were also collected in fluvial deposits at Arlanzón (Burgos, Spain). Type Q2 is characterized by a grey matrix with reddish oxide bands. Type Q3 is characterized by a dark blue color and being much more fine grained than the two previous types, although some internal fissures show a minor presence of oxides. Three flakes of F1, F2, Q1 and Q2 were selected, while four flakes were selected for F3 and Q3. This makes for a total of ten flakes of flint and ten flakes of quartzite.

2.2 Image capturing workflow

The present work takes a series of steps prior to realizing any analysis and extracting data from images. These steps are: the cleaning protocol to remove contaminants, image capture, and image enhancement.

2.2.1 Cleaning protocol Multiple works emphasize the need of cleaning protocols to remove modern contaminants prior to analysis ([Asryan and Ollé, 2020](#); [Fernández-Marchena and Ollé, 2016](#); [Ollé and Vergès, 2014](#); [Pedergnana et al., 2016](#)). Figure @ref(fig:Figure-01) shows the effect of manual manipulation on the texture of a surface. Because of this, a multi-step procedure based on previous studies was adopted ([Pedergnana et al., 2016](#)). This multi-step procedure included a sonic bath in 2% neutral soap (Derquim) solution during 10 to 15 minutes. This was followed by a second sonic bath in pure acetone during another 10 to 15 minutes. After each step the lithic artefacts were introduced in a water bath and finally dried using pressure air. During the cleaning protocol and microscopic analysis all artefacts were manipulated using surgical gloves.

2.2.2 Image capture Dino-Lite Edge 3.0 AM73915MZT USB microscope
-capsule vertical stand -pelota esa

2.2.3 Image enhancement A common problem of images obtained from USB microscopes is the lack of detail due to saturation in one of the grey level values and effects of different lightning. This saturation is often observed as a general glaze in one of the grey level values and results in a low quality image with poor detail. To increase detail and quality prior to the analysis, all images were subjected to a two-step process. First, the Fiji plugging *Subtract background* was employed to avoid effects of different lightning. Second, the function *enhance contrast* was employed to desaturize the images by normalizing their histograms (Figure @ref(fig:Figure3)).

2.3 Image statistical analysis

The present work uses three sets of statistical metrics to analyze obtained images. The first set of statistical metrics correspond to descriptive statistics (mean, standard deviation, mode, median and kurtosis). The second set of statistical measures corresponds to measures of roughness:

- **Root mean square deviation (Rq):** indicator of surface roughness.
- **Arithmetical mean deviation (Ra):** which indicates the deviation of a surface from a mean height.

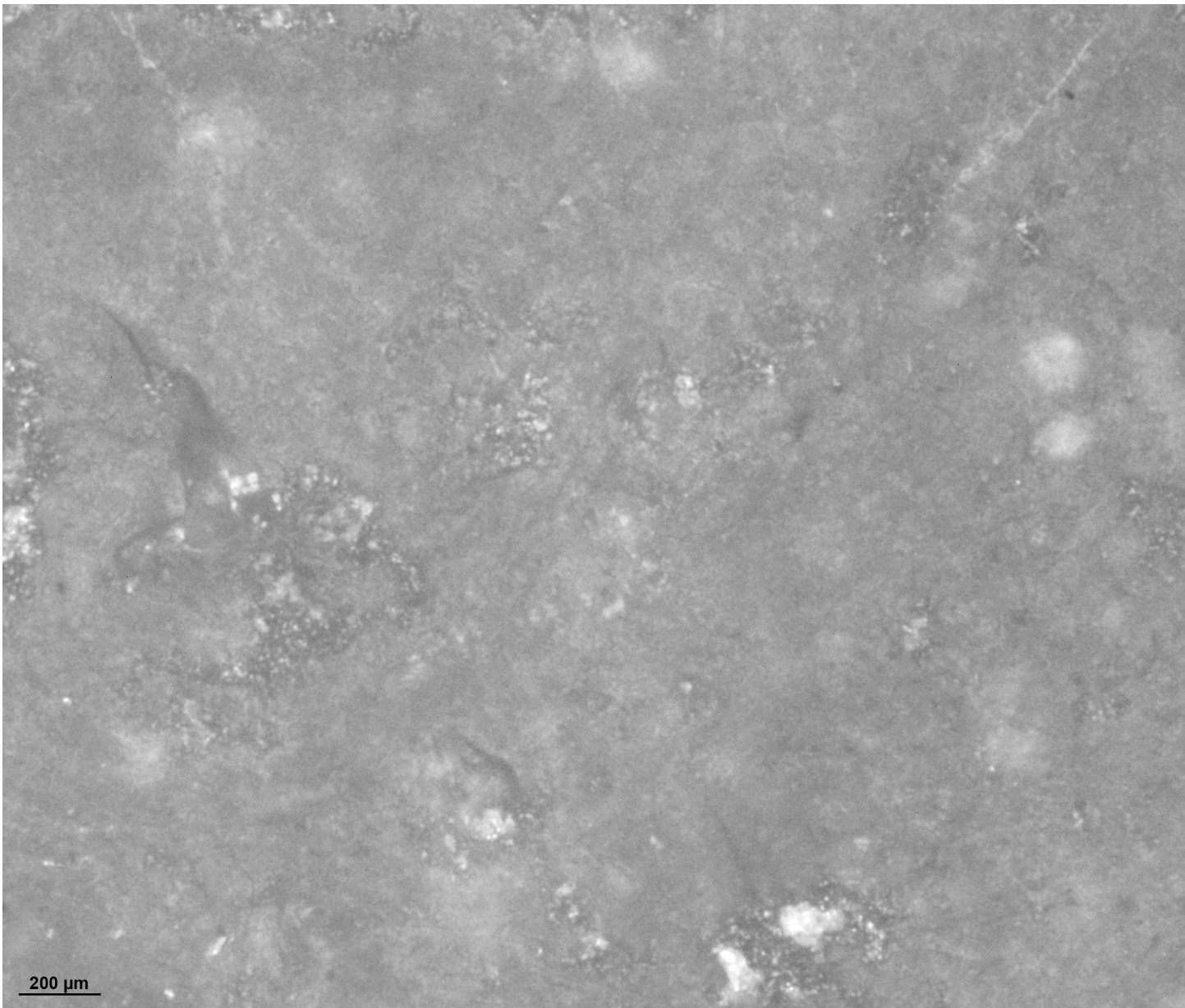


Figure 1: Effects of manual manipulation without protection on flint surface. Left: surface photographed after the application of cleaning protocol and manipulation of the artefact using protection. Right: same surface after manual manipulation without protection.

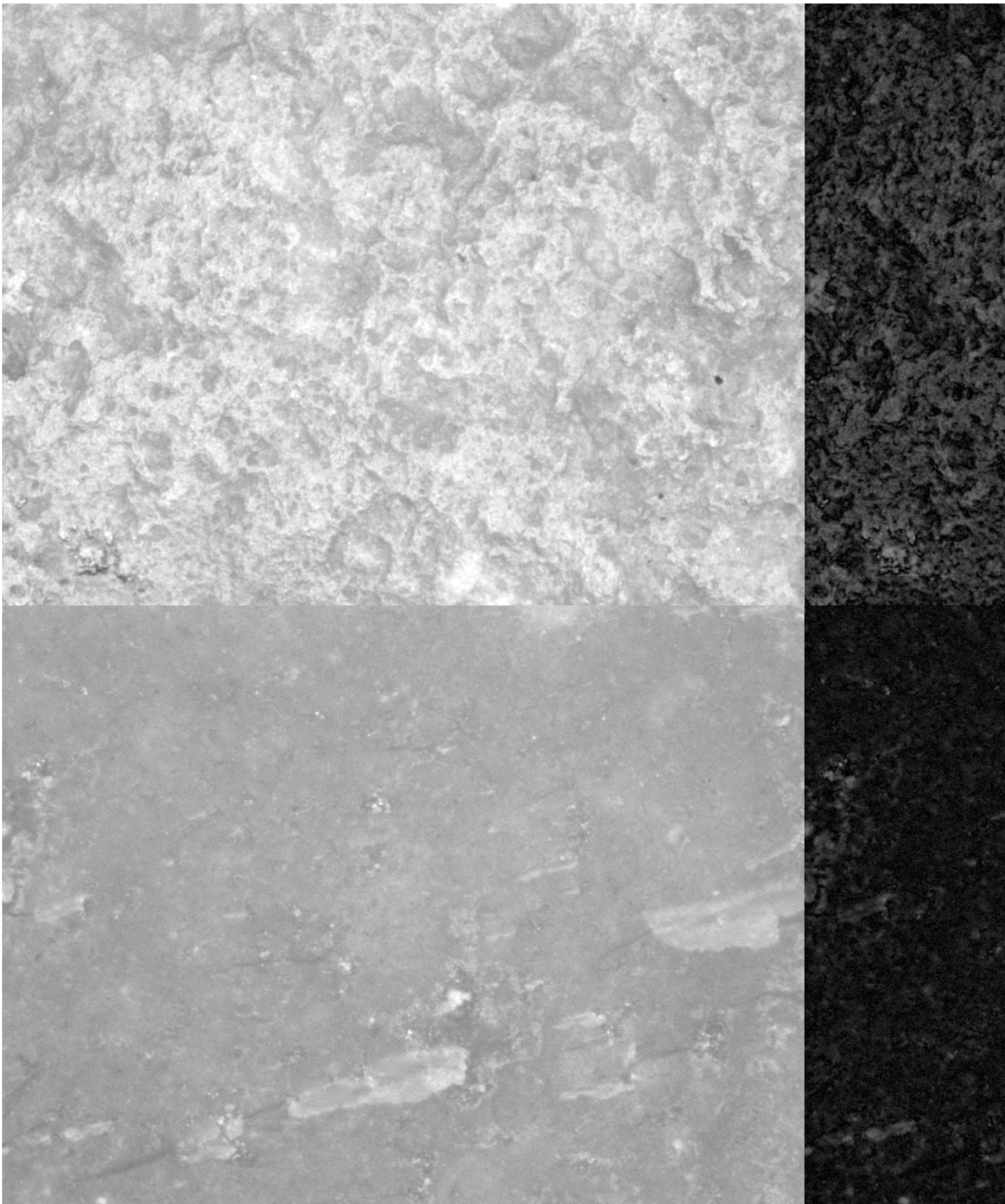


Figure 2: Two examples of image enhancement. Left: original images taken by a digital microscope. Center: images after retrieving the background to avoid effects of different lighting. Right: after normalizing the histogram to avoid saturation and increase detail. Top row: geological neocortex. Bottom row: fresh surface of experimentally knapped flake.

- **Skewness of the assessed profile (Rsk):** indicator of the departure from surface symmetry. Negative values indicate a surface made of deep valey, and positive values indicates peaks and asperities.
- **Kurtosis of the assessed profile (Rku):** which indicates the sharpness of the peaks. Low values indicate blunt peaks, while high values indicate sharp peaks.

The implementation of these measures is done in ImageJ software ([Schneider et al., 2012](#)) through the Roughness calculation plugin ([Chinga and Dougherty, 2002](#)).

A problem exists when images are analyzed through the intensity distribution of pixels and using descriptive statistics and roughness metrics. Figure @ref(fig:Figure2) illustrates the problem. Figure @ref(fig:Figure2) shows a series of pattern images with similar values of intensity, but with different spatial distribution. Regarding descriptive statistics, all images present similar values of mean (127), standard deviation (125), sk (0.01) and kurtosis (-1.99). Regarding measures of roughness, all images present similar values of Rq (180), Ra (127), Rsk (1.42), and Rku (2).

Analysis of intensity values through the Gray Level Co-occurrence Matrix (GLCM; [Haralick et al. \(1973\)](#)) takes into consideration the spatial distribution of intensity values. The GLCM works in two steps ([Haralick et al., 1973](#)). First, using a given distance and direction (@ref(fig:Scheme-GLCM)), it builds a matrix which captures the relationship of intensity between pairs of pixels (reference and neighbor). Second, for every x and y it considers the co-occurrence of values, forming a new matrix. From this new matrix, a series of statistical descriptors are derived ([Haralick et al., 1973](#)).

- **Angular Second Moment (ASM)** is measure of homogeneity in the image. Homogeneous images (with low gray-tone transitions) will have fewer entries of large magnitude. Thus homogeneous images will have high ASM values, while the opposite will be true for non-homogeneous images.
- **Contrast (CONT)** is a value of the amount of local variations, with high values indicating a lot of local variation and low values few local variation.
- **Correlation (CORR)** which measures gray-tone linear-dependencies in the image. It indicates how a reference pixel is related to its neighbor. A 0 value indicates it is uncorrelated, and 1 indicates a perfect correlation.
- **Inverse Different Moment (IDM)** also referred as **homogeneity**. It obtains the measures of the closeness of the distribution of the GLCM elements to the GLCM diagonal.
- **Entropy (ENT):** is a measure of the amount of irremediable chaos or disorder in an image. High values of entropy indicate values of similar magnitude, while low values indicate unequal entries.

Figure @ref(fig:PatternFig-Box) shows results from the application of [Haralick et al. \(1973\)](#) textural features to the same pattern images.

```
library(tidyverse)
# GLCM of sequential data
GLCM.txt <- read.delim("Data/Pattern_GLCM.txt", sep = ",")  
  

GLCM.txt <- GLCM.txt %>% filter(
  !grepl("#", X.)) %>%
  mutate(Angular.Second.Moment = as.numeric(Angular.Second.Moment),
        Contrast = as.numeric(Contrast),
        Correlation = as.numeric(Correlation),
```

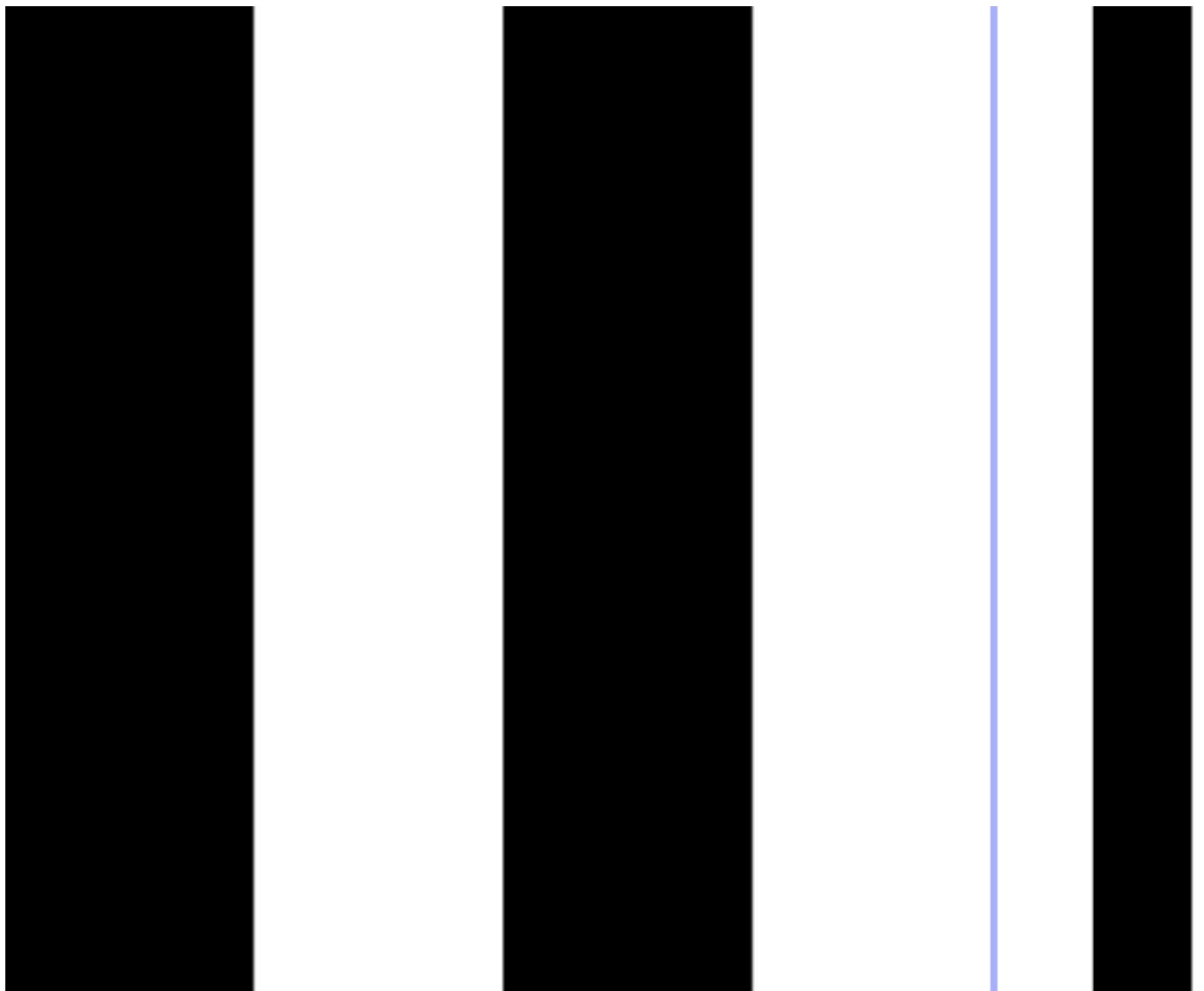


Figure 3: Pattern figures presenting similar intensity distribution values, but a different spatial distribution

		2		
		1		
2	1	I,J	1	2
		1		
		2		

Figure 4: Basic representation of how the GLCM takes into consideration the spatial relationships of pixels and intensity value. The spatial relationships are considered given a reference pixel (I,J), a direction (north, east, south or west), and a distance (one pixel, two pixels)

```

Inverse.Difference.Moment = as.numeric(Inverse.Difference.Moment),
Entropy = as.numeric(Entropy)
) %>%
rename(ID = X.) %>%
select(-c(X)) %>%
group_by(ID) %>%
summarise(
  ASM = mean(Angular.Second.Moment),
  CONT = mean(Contrast),
  CORR = mean(Correlation),
  IDM = mean(Inverse.Difference.Moment),
  ENT = mean(Entropy)
) %>%
mutate(
  ID = substring(ID, 3)) %>%
mutate(
  ID = substring(ID, 1, nchar(ID)-5))

```

```

GLCM.txt %>% pivot_longer(
  cols = ASM:ENT,
  names_to = "Variable",
  values_to = "values") %>%

ggplot(aes("Variable", values, label = ID)) +
  facet_wrap(~ Variable, scales = "free",
             ncol = 2) +
  xlab(NULL) +
  ylab(NULL) +

```

```

geom_jitter(aes(color = ID),
            width = 0.1, shape = 18, size = 3) +
ggrepel::geom_text_repel() +
ggsci::scale_color_jco() +
theme_light() +
theme(
  axis.text.x = element_blank(),
  strip.text = element_text(color = "black", face = "bold", size = 11),
  strip.background = element_rect(fill = "white", colour = "black", size = 1),
  axis.text = element_text(color = "black"),
  legend.position = "none")

```

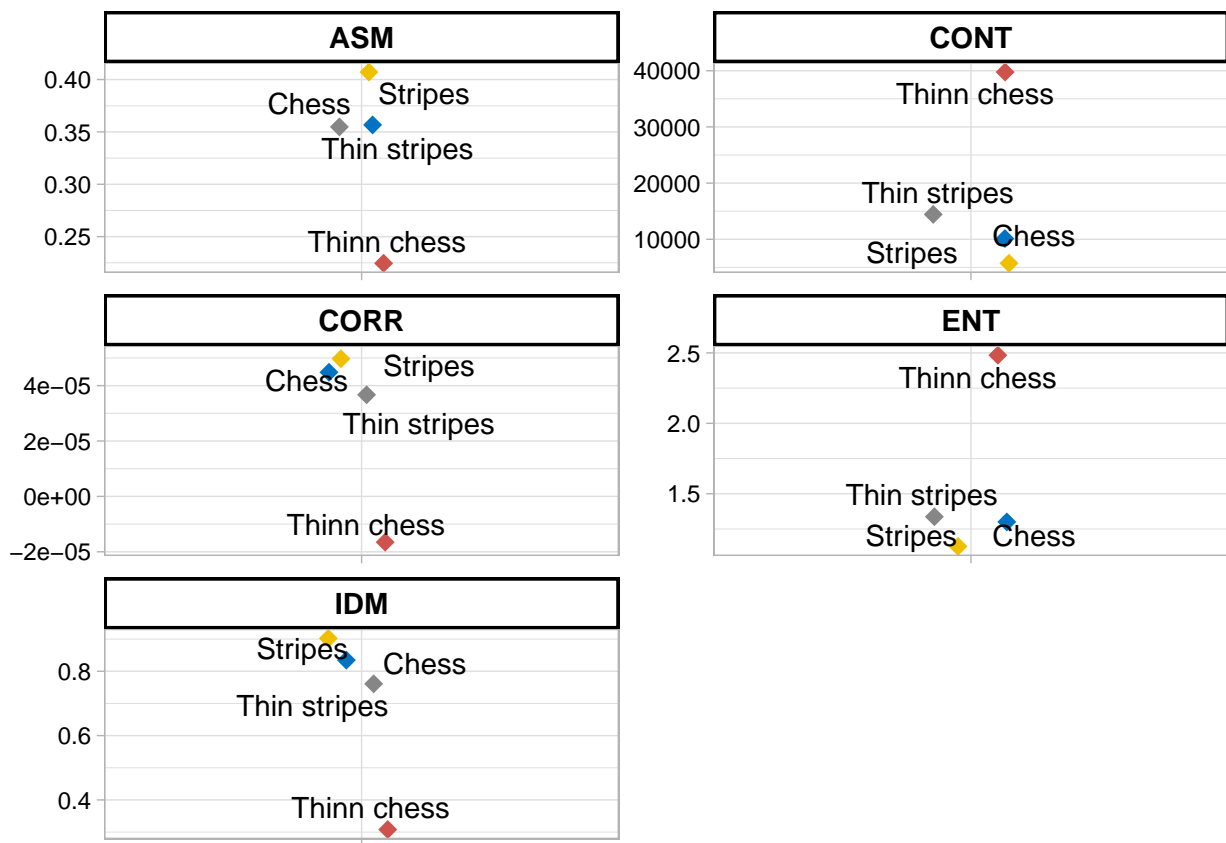


Figure 5: Values of pattern images using Haralick et al 1973 GLCM and second order statistics

The present work implements Haralick et al. (1973) analysis and metrics in ImageJ software (Schneider et al., 2012). Calculation of GLCM and second order statistics is done through Cabrera (2006) plugin.

2.4 Proof of Concept of GLCM and texture analysis

Prior to the application of Haralick et al. (1973) texture metrics a proof of concept from a pilot study is undertaken. This proof of concept is aimed to two objectives. First, determine if the GLCM provides suitable variable values to discriminate between degrees of sedimentary abrasion. Second, to determine to the best interval of pixels under which the GLCM works

The proof of concept sample is composed of 23 images corresponding to geological neocortex, 56 images corresponding to flakes undergone 10 hours of sedimentary abrasion in a previous experimental study (Bustos-Pérez et al., 2019) and 42 images corresponding to fresh surfaces from experimentally knapped flakes. All flints correspond to South Madrid Miocene Flint (Bustillo and Pérez-Jiménez (2005); Bustillo et al. (2012)).

The GLCM requires to test for several distances between the reference pixel and the neighboring pixel on which the spatial relationships are established. The present work tests for five different sequences of distances (Table @ref(tab:distances)). The first sequence composes the GLCM based on pixels located at distances 1, 2, 3 and 4 from the reference pixel. Sequence 2 composes the GLCM based on pixels located at distances 2, 4, 6 and 8 from the reference pixel (Table @ref(tab:distances)). All sequences of intervals are tested in the four cardinal directions (north, east, south and west). This results in 16 (four per each cardinal direction) values of Haralick et al. (1973) textural metrics. Final values are obtained by averaging the different values of each of the variables although range is not considered (Bietti, 1996).

Table 1: Sequences and distance of pixels considerer.

Sequence	Pixel Distances
1	1-2-3-4
2	2-4-6-8
3	5-10-15-20
4	10-20-30-40
5	50-100-150-200

```
load("Data/PoC Data.RData")
```

References

- Alhusban, Z., Valyrakis, M., 2021. Assessing and Modelling the Interactions of Instrumented Particles with Bed Surface at Low Transport Conditions. *Applied Sciences* 11, 7306. <https://doi.org/10.3390/app11167306>
- Asryan, L., Ollé, A., 2020. Results of a functional study on the Middle to early Upper Pleistocene lithic assemblages from the Azokh 1 Cave site (South Caucasus). *Quaternary International* 569-570, 168–180. <https://doi.org/10.1016/j.quaint.2020.05.028>
- Bertran, P., Lenoble, A., Todisco, D., Desrosiers, P.M., Sørensen, M., 2012. Particle size distribution of lithic assemblages and taphonomy of Palaeolithic sites. *Journal of Archaeological Science* 39, 3148–3166. <https://doi.org/10.1016/j.jas.2012.04.055>
- Bietti, A., 1996. Image processing in microwear studies of flint artifacts. *Archeologi e Calcolatori* 7, 387–396.
- Bustillo, M.A., Pérez-Jiménez, J.L., 2005. Características diferenciales y génesis de los niveles silíceos explotados en el yacimiento arqueológico de Casa Montero (Vicálvaro, Madrid). *Geogaceta* 38, 243–246.
- Bustillo, M.Á., Pérez-Jiménez, J.L., Bustillo, M., 2012. Caracterización geoquímica de rocas sedimentarias formadas por silicificación como fuentes de suministro de utensilios líticos (Mioceno, cuenca de Madrid). *Revista Mexicana de Ciencias Geológicas* 29, 233–247.
- Bustos-Pérez, G., Díaz, S., Baena, J., 2019. An Experimental Approach to Degrees of Rounding Among Lithic Artifacts. *Journal of Archaeological Method and Theory* 26, 1243–1275. <https://doi.org/10.1007/s10816-018-9409-8>
- Cabrera, J.E., 2006. Texture Analyzer.
- Chambers, J.C., 2003. Like a rolling stone? The identification of fluvial transportation damage signatures on secondary context bifaces. *Lithics* 24, 66–77.
- Chinga, G., Dougherty, B., 2002. Roughness Calculation.
- Chu, W., Thompson, C., Hosfield, R., 2015. Micro-abrasion of flint artifacts by mobile sediments: A taphonomic approach. *Archaeological and Anthropological Sciences* 7, 3–11. <https://doi.org/10.1007/s12520-013-0157-0>

- Fernández-Marchena, J.L., Ollé, A., 2016. Microscopic analysis of technical and functional traces as a method for the use-wear analysis of rock crystal tools. *Quaternary International* 424, 171–190. <https://doi.org/10.1016/j.quaint.2015.10.064>
- Haralick, R.M., Shanmugam, K., Dinstein, I.H., 1973. Textural features for image classification. *IEEE Transactions on systems, man, and cybernetics* 3, 610–621.
- Harding, P., Gibbard, P.L., Lewin, J., Macklin, M.G., Moss, E.H., 1987. The transport and abrasion of flint handaxes in a gravel-bed river, in: Sieveking, G., Newcomer, M. (Eds.), *The Human Uses of Flint and Chert: Proceedings of the Fourth International Flint Symposium Held at Brighton Polytechnic*. Cambridge University Press, Cambridge, pp. 115–126.
- Lenoble, A., Bertran, P., 2004. Fabric of Palaeolithic levels: Methods and implications for site formation processes. *Journal of Archaeological Science* 31, 457–469. <https://doi.org/10.1016/j.jas.2003.09.013>
- Levi Sala, I., 1986. Use Wear and Post-depositional Surface Modification: A Word of Caution. *Journal of Archaeological Science* 13, 229–244.
- Luedtke, B.E., 1992. An Archaeologist's Guide to Chert and Flint, *Archaeological Research Tools*. Institute of Archaeology, University of California, Los Angeles.
- Maillo Fernández, J.M., 1998. Proporciones de debris en réplicas de talla experimental. *Espacio Tiempo y Forma. Serie I, Prehistoria y Arqueología*. <https://doi.org/10.5944/etfi.11.1998.4665>
- McPherron, S.J.P., 2005. Artifact orientations and site formation processes from total station proveniences. *Journal of Archaeological Science* 32, 1003–1014.
- McPherron, S.P., 2018. Additional statistical and graphical methods for analyzing site formation processes using artifact orientations. *PLOS ONE* 13, e0190195. <https://doi.org/10.1371/journal.pone.0190195>
- Ollé, A., Vergès, J.M., 2014. The use of sequential experiments and SEM in documenting stone tool microwear. *Journal of Archaeological Science* 48, 60–71. <https://doi.org/10.1016/j.jas.2013.10.028>
- Pedergnana, A., Asryan, L., Fernández-Marchena, J.L., Ollé, A., 2016. Modern contaminants affecting microscopic residue analysis on stone tools: A word of caution. *Micron* 86, 1–21. <https://doi.org/10.1016/j.micron.2016.04.003>
- Petraglia, M.D., Potts, R., 1994. Water Flow and the Formation of Early Pleistocene Artifact Sites in Olduvai Gorge, Tanzania. *Journal of Anthropological Archaeology* 13, 228–254. <https://doi.org/10.1006/jaar.1994.1014>
- Schick, K.D., 1987. Modeling the formation of Early Stone Age artifact concentrations. *Journal of Human Evolution* 16, 789–807. [https://doi.org/10.1016/0047-2484\(87\)90024-8](https://doi.org/10.1016/0047-2484(87)90024-8)
- Schick, K.D., 1986. Stone Age sites in the making: Experiments in the formation and transformation of archaeological occurrences, *BAR International Series*. BAR Publishing, Oxford.
- Schiffer, M.B., 1972. Archaeological Context and Systemic Context. *American Antiquity* 37, 156–165. <https://doi.org/10.2307/278203>
- Schneider, C.A., Rasband, W.S., Eliceiri, K.W., 2012. NIH Image to ImageJ: 25 years of image analysis. *Nature Methods* 9, 671–675. <https://doi.org/10.1038/nmeth.2089>
- Shackley, M.S., 1974. Stream abrasion of flint implements. *Nature* 248, 501–502.
- Stapert, D., 1976. Some natural surface modifications on flint in the Netherlands. *Paleohistoria* 18, 9–41.